Observation of $e^+e^- \to pp\bar{p}\bar{n}\pi^- + c.c.$

M. Ablikim¹, M. N. Achasov^{11,b}, P. Adlarson⁷⁰, M. Albrecht⁴, R. Aliberti³¹, A. Amoroso^{69A,69C}, M. R. An³⁵, Q. An^{53,66}, X. H. Bai⁶¹, Y. Bai⁵², O. Bakina³², R. Baldini Ferroli^{26A}, I. Balossino^{27A,1}, Y. Ban^{42,g}, V. Batozskaya^{1,40}, D. Becker³¹, K. Begzsuren²⁹, N. Berger³¹, M. Bertani^{26A}, D. Bettoni^{27A}, F. Bianchi^{69A,69C}, J. Bloms⁶³, A. Bortone^{69A,69C}, I. Boyko³², R. A. Briere⁵, A. Brueggemann⁶³, H. Cai⁷¹, X. Cai^{1,53}, A. Calcaterra^{26A}, G. F. Cao^{1,58}, N. Cao^{1,58}, S. A. Cetin^{57A}, J. F. Chang^{1,53}, W. L. Chang^{1,58}, G. Chelkov^{32,a}, C. Chen³⁹, Chao Chen⁵⁰, G. Chen¹, H. S. Chen^{1,58}, M. L. Chen^{1,53}, S. J. Chen³⁸, S. M. Chen⁵⁶, T. Chen¹, X. R. Chen^{28,58}, X. T. Chen¹, Y. B. Chen^{1,53}, Z. J. Chen^{23,h}, W. S. Cheng^{69C}, X. Chu³⁹, G. Cibinetto^{27A}, F. Cossio^{69C}, J. J. Cui⁴⁵, H. L. Dai^{1,53}, J. P. Dai⁷³, A. Dbeyssi¹⁷, R. E. de Boer⁴, D. Dedovich³², Z. Y. Deng¹, A. Denig³¹, I. Denysenko³², M. Destefanis^{69A,69C}, F. De Mori^{69A,69C}, Y. Ding³⁶, J. Dong^{1,53}, L. Y. Dong^{1,58}, M. Y. Dong¹, X. Dong⁷¹, S. X. Du⁷⁵, P. Egorov^{32,a}, Y. L. Fan⁷¹, J. Fang^{1,53}, S. S. Fang^{1,58}, W. X. Fang¹, Y. Fang¹, R. Farinelli^{27A}, L. Fava^{69B,69C}, F. Feldbauer⁴, G. Felici^{26A}, C. Q. Feng^{53,66}, J. H. Feng⁵⁴, K Fischer⁶⁴, M. Fritsch⁴, C. Fritzsch⁶³, C. D. Fu¹, H. Gao⁵⁸, Y. N. Gao^{42,9}, Yang Gao^{53,66}, S. Garbolino^{69C}, I. Garzia^{27A,27B}, P. T. Ge⁷¹, Z. W. Ge³⁸, C. Geng⁵⁴, E. M. Gersabeck⁶², A Gilman⁶⁴, K. Goetzen¹², L. Gong³⁶, W. X. Gong^{1,53}, W. Gradl³¹, M. Greco^{69A,69C}, L. M. Gu³⁸, M. H. Gu^{1,53}, Y. T. Gu¹⁴, C. Y Guan^{1,58}, A. Q. Guo^{28,58}, L. B. Guo³⁷, R. P. Guo⁴⁴, Y. P. Guo^{10,f}, A. Guskov^{32,a}, T. T. Han⁴⁵, W. Y. Han³⁵, X. Q. Hao¹⁸, F. A. Harris⁶⁰, K. K. He⁵⁰, K. L. He^{1,58}, F. H. Heinsius⁴, C. H. Heinz³¹, Y. K. Heng¹, C. Herold⁵⁵, M. Himmelreich^{12,d}, G. Y. Hou^{1,58}, Y. R. Hou⁵⁸, Z. L. Hou¹, H. M. Hu^{1,58} J. F. Hu^{51,i}, T. Hu¹, Y. Hu¹, G. S. Huang^{53,66}, K. X. Huang⁵⁴, L. Q. Huang⁶⁷, L. Q. Huang^{28,58}, X. T. Huang⁴⁵, Y. P. Huang¹, Z. Huang^{42,9}, T. Hussain⁶⁸, N Hüsken^{25,31}, W. Imoehl²⁵, M. Irshad^{53,66}, J. Jackson²⁵, S. Jaeger⁴, S. Janchiv²⁹, Q. Ji¹, Q. P. Ji¹⁸, X. B. Ji^{1,58}, X. L. Ji^{1,53}, Y. Y. Ji⁴⁵, Z. K. Jia^{53,66}, H. B. Jiang⁴⁵, S. S. Jiang³⁵, X. S. Jiang¹, Y. Jiang⁵⁸, J. B. Jiao⁴⁵, Z. Jiao²¹, S. Jin³⁸, Y. Jin⁶¹, M. Q. Jing^{1,58}, T. Johansson⁷⁰, N. Kalantar-Nayestanaki⁵⁹, X. S. Kang³⁶, R. Kappert⁵⁹, B. C. Ke⁷⁵, I. K. Keshk⁴, A. Khoukaz⁶³, P. Kiese³¹, R. Kiuchi¹, R. Kliemt¹², L. Koch³³, O. B. Kolcu^{57A}, B. Kopf⁴, M. Kuemmel⁴, M. Kuessner⁴, A. Kupsc^{40,70}, W. Kühn³³, J. J. Lane⁶², J. S. Lange³³, P. Larin¹⁷, A. Lavania²⁴, L. Lavezzi^{69A,69C}, Z. H. Lei^{53,66}, H. Leithoff³¹, M. Lellmann³¹, T. Lenz³¹, C. Li⁴³, C. Li³⁹, C. H. Li³⁵, Cheng Li^{53,66}, D. M. Li⁷⁵, F. Li^{1,53}, G. Li¹, H. Li⁴⁷, H. Li^{53,66}, H. B. Li^{1,58}, H. J. Li¹⁸, H. N. Li^{51,i}, J. Q. Li⁴, J. S. Li⁵⁴, J. W. Li⁴⁵, Ke Li¹, L. J Li¹, L. K. Li¹, Lei Li³, M. H. Li³⁹, P. R. Li^{34,j,k}, S. X. Li¹⁰, S. Y. Li⁵⁶, T. Li⁴⁵, W. D. Li^{1,58}, W. G. Li¹, X. H. Li^{53,66}, X. L. Li⁴⁵, Xiaoyu Li^{1,58}, H. Liang^{53,66}, H. Liang^{1,58}, H. Liang³⁰, Y. F. Liang⁴⁹, Y. T. Liang^{28,58}, G. R. Liao¹³, L. Z. Liao⁴⁵, J. Libby²⁴, A. Limphirat⁵⁵, C. X. Lin⁵⁴, D. X. Lin^{28,58}, T. Lin¹, B. J. Liu¹, C. X. Liu¹, D. Liu^{17,66}, F. H. Liu⁴⁸, Fang Liu¹, Feng Liu⁶, G. M. Liu^{51,i}, H. Liu^{34,j,k}, H. B. Liu¹⁴, H. M. Liu^{1,58}, Huanhuan Liu¹, Huihui Liu¹⁹, J. B. Liu^{53,66}, J. L. Liu⁶⁷, Feng Liu⁵, G. M. Liu^{5,7}, H. Liu^{5,7}, H. B. Liu⁷, H. M. Liu^{1,7}, Huannuan Liu , Humui Liu , J. B. Liu , J. Y. Liu^{1,58}, K. Liu¹, K. Y. Liu³⁶, Ke Liu²⁰, L. Liu^{53,66}, Lu Liu³⁹, M. H. Liu^{10,f}, P. L. Liu¹, Q. Liu⁵⁸, S. B. Liu^{53,66}, T. Liu^{10,f}, W. K. Liu³⁹, W. M. Liu^{53,66}, X. Liu^{34,j,k}, Y. Liu^{34,j,k}, Y. B. Liu³⁹, Z. A. Liu¹, Z. Q. Liu⁴⁵, X. C. Lou¹, F. X. Lu⁵⁴, H. J. Lu²¹, J. G. Lu^{1,53}, X. L. Lu¹, Y. Lu⁷, Y. P. Lu^{1,53}, Z. H. Lu¹, C. L. Luo³⁷, M. X. Luo⁷⁴, T. Luo^{10,f}, X. L. Luo^{1,53}, X. R. Lyu⁵⁸, Y. F. Lyu³⁹, F. C. Ma³⁶, H. L. Ma¹, L. L. Ma⁴⁵, M. M. Ma^{1,58}, Q. M. Ma¹, R. Q. Ma^{1,58}, R. T. Ma⁵⁸, X. Y. Ma^{1,53}, Y. Ma^{42,9}, F. E. Maas¹⁷, M. Maggiora^{69,69C}, S. Maldaner⁴, S. Malde⁶⁴, Q. A. Malik⁶⁸, A. Mangoni^{26B}, Y. J. Mao^{42,g}, Z. P. Mao¹, S. Marcello^{69A,69C}, Z. X. Meng⁶¹, J. G. Messchendorp⁵⁹, G. Mezzadri^{27A,1}, H. Miao¹, T. J. Min³⁸, R. E. Mitchell 25 , X. H. Mo 1 , N. Yu. Muchnoi 11,b , Y. Nefedov 32 , F. Nerling 17,d , I. B. Nikolaev 11,b , Z. Ning 1,53 , S. Nisar 9,l , Y. Niu⁴⁵, S. L. Olsen⁵⁸, Q. Ouyang¹, S. Pacetti^{26B,26C}, X. Pan^{10,f}, Y. Pan⁵², A. Pathak³⁰, M. Pelizaeus⁴, H. P. Peng^{53,66} K. Peters^{12,d}, J. L. Ping³⁷, R. G. Ping^{1,58}, S. Plura³¹, S. Pogodin³², V. Prasad^{53,66}, F. Z. Qi¹, H. Qi^{53,66}, H. R. Qi⁵⁶, M. Qi³⁸, T. Y. Qi^{10,f}, S. Qian^{1,53}, W. B. Qian⁵⁸, Z. Qian⁵⁴, C. F. Qiao⁵⁸, J. J. Qin⁶⁷, L. Q. Qin¹³, X. P. Qin^{10,f}, X. S. Qin⁴⁵, Z. H. Qin^{1,53}, J. F. Qiu¹, S. Q. Qu⁵⁶, K. H. Rashid⁶⁸, C. F. Redmer³¹, K. J. Ren³⁵, A. Rivetti^{69C}, V. Rodin⁵⁹, M. Rolo^{69C}, G. Rong^{1,58}, Ch. Rosner¹⁷, S. N. Ruan³⁹, H. S. Sang⁶⁶, A. Sarantsev^{32,c}, Y. Schelhaas³¹, C. Schnier⁴, K. Schoenning⁷⁰, M. Scodeggio^{27A,27B}, K. Y. Shan^{10,f}, W. Shan²², X. Y. Shan^{53,66}, J. F. Shangguan⁵⁰, L. G. Shao^{1,58}, M. Shao^{53,66}, C. P. Shen^{10,f}, H. F. Shen^{1,58}, X. Y. Shen^{1,58}, B. A. Shi⁵⁸, H. C. Shi^{53,66}, J. Y. Shi¹, Q. Q. Shi⁵⁰, R. S. Shi^{1,58}, X. Shi^{1,53}, X. D Shi^{53,66}, J. J. Song¹⁸, W. M. Song^{1,30}, Y. X. Song^{42,9}, S. Sosio^{69A,69C}, S. Spataro^{69A,69C}, F. Stieler³¹, K. X. Su⁷¹, P. P. Su⁵⁰, Y. J. Su⁵⁸, G. X. Sun¹, H. Sun⁵⁸, H. K. Sun¹, J. F. Sun¹⁸, L. Sun⁷¹, S. S. Sun^{1,58}, T. Sun^{1,58}, W. Y. Sun³⁰,

Received xxxx june xxxx

^{*} This work is supported in part by National Key R&D Program of China under Contracts Nos. Supported in part by National Key R&D Program of China under Contracts Nos. 2020YFA0406300, 2020YFA0406400; National Natural Science Foundation of China (NSFC) under Contracts Nos. 11975118, 11625523, 11635010, 11735014, 11822506, 11835012, 11935015, 11935016, 11935018, 11961141012, 12022510, 12025502, 12035009, 12035013, 12061131003, 12075252, 12192260, 12192261, 12192262, 12192263, 12192264, 12192265; the Natural Science Foundation of Hunan Province of China under Contract No. 2019JJ30019; the Science and Technology Innovation Program of Hunan Province under Contract No. 2020RC3054; the Chinese Academy of Sciences (CAS) Large-Scale Scientific Facility Program; Joint Large-Scale Scientific Facility Funds of the NSFC and CAS under Contracts Nos. U1732263, U1832207; CAS Key Research Program of Frontier Sciences under Contract No. QYZDJ-SSW-SLH040; 100 Talents Program of CAS; INPAC and Shanghai Key Laboratory for Particle Physics and Cosmology; ERC under Contract No. 758462; European Union Horizon 2020 research and innovation programme under Contract No. Marie Sklodowska-Curie grant agreement No. 894790; German Research Foundation DFG under Contracts Nos. 443159800, Collaborative Research Center CRC 1044, FOR 2359, GRK 2149; Istituto Nazionale di Fisica Nucleare, Italy; Ministry of Development of Turkey under Contract No. DPT2006K-120470; National Science and Technology fund; Olle Engkvist Foundation under Contract No. 200-0605; STFC (United Kingdom); The Knut and Alice Wallenberg Foundation (Sweden) under Contract No. 2016.0157; The Royal Society, UK under Contracts Nos. DH140054, DH160214; The Swedish Research Council; U. S. Department of Energy under Contracts Nos. DE-FG02-05ER41374, DE-SC-0012069.

X Sun^{23,h}, Y. J. Sun^{53,66}, Y. Z. Sun¹, Z. T. Sun⁴⁵, Y. H. Tan⁷¹, Y. X. Tan^{53,66}, C. J. Tang⁴⁹, G. Y. Tang¹, J. Tang⁵⁴, L. Y Tao⁶⁷, Q. T. Tao^{23,h}, M. Tat⁶⁴, J. X. Teng^{53,66}, V. Thoren⁷⁰, W. H. Tian⁴⁷, Y. Tian^{28,58}, I. Uman^{57B}, B. Wang¹, B. L. Wang⁵⁸, C. W. Wang³⁸, D. Y. Wang^{42,9}, F. Wang⁶⁷, H. J. Wang^{34,j,k}, H. P. Wang^{1,58}, K. Wang^{1,53}, L. L. Wang¹, M. Wang⁴⁵, M. Z. Wang^{42,9}, Meng Wang^{1,58}, S. Wang¹³, S. Wang^{10,f}, T. Wang^{10,f}, T. J. Wang³⁹, W. Wang⁵⁴, W. H. Wang⁷¹, W. P. Wang^{53,66}, X. Wang^{42,9}, X. F. Wang^{34,j,k}, X. L. Wang^{10,f}, Y. Wang⁵⁶, Y. D. Wang⁴¹, Y. F. Wang¹, Y. H. Wang⁴³, Y. Q. Wang¹, Yaqian Wang^{1,16}, Z. Wang^{1,53}, Z. Y. Wang^{1,58}, Ziyi Wang⁵⁸, D. H. Wei¹³, F. Weidner⁶³, S. P. Wen¹, D. J. White⁶², U. Wiedner⁴, G. Wilkinson⁶⁴, M. Wolke⁷⁰, L. Wollenberg⁴, J. F. Wu^{1,58}, L. H. Wu¹, L. J. Wu^{1,58}, X. Wu^{10,f}, X. H. Wu³⁰, Y. Wu⁶⁶, Z. Wu^{1,53}, L. Xia^{53,66}, T. Xiang^{42,g}, D. Xiao^{34,j,k}, G. Y. Xiao³⁸, H. Xiao^{10,f}, S. Y. Xiao¹, Y. L. Xiao^{10,f}, Z. J. Xiao³⁷, C. Xie³⁸, X. H. Xie^{42,g}, Y. Xie⁴⁵, Y. G. Xie^{1,53}, Y. H. Xie⁶, Z. P. Xie^{53,66}, T. Y. Xing^{1,58}, C. F. Xu¹, C. J. Xu⁵⁴, G. F. Xu¹, H. Y. Xu⁶¹, Q. J. Xu¹⁵, X. P. Xu⁵⁰, Y. C. Xu⁵⁸, Z. P. Xu³⁸, F. Yan^{10,f}, L. Yan^{10,f}, W. B. Yan^{53,66}, W. C. Yan⁷⁵, H. J. Yang^{46,e}, H. L. Yang³⁰, H. X. Yang¹, L. Yang⁴⁷, S. L. Yang⁵⁸, Tao Yang¹, Y. F. Yang³⁹, Y. X. Yang^{1,58}, Yifan Yang^{1,58}, M. Ye^{1,53}, M. H. Ye⁸, J. H. Yin¹, Z. Y. You⁵⁴, B. X. Yu¹, C. X. Yu³⁹, G. Yu^{1,58}, T. Yu⁶⁷, C. Z. Yuan^{1,58}, L. Yuan², S. C. Yuan¹, X. Q. Yuan¹, Y. Yuan^{1,58}, Z. Y. Yuan⁵⁴, C. X. Yue³⁵, A. A. Zafar⁶⁸, F. R. Zeng⁴⁵, X. Zeng⁶, Y. Zeng^{23,h}, Y. H. Zhan⁵⁴, A. Q. Zhang¹, B. L. Zhang¹, B. X. Zhang¹, D. H. Zhang³⁹, G. Y. Zhang¹⁸, H. Zhang⁶⁶, H. H. Zhang⁵⁴, H. H. Zhang³⁰, H. Y. Zhang^{1,53}, J. L. Zhang⁷², J. Q. Zhang³⁷, J. W. Zhang¹, J. X. Zhang^{34,j,k}, J. Y. Zhang¹, J. Z. Zhang^{1,58}, Jianyu Zhang^{1,58}, Jiawei Zhang^{1,58}, L. M. Zhang⁵⁶, L. Q. Zhang⁵⁴, Lei Zhang³⁸, P. Zhang¹, Q. Y. Zhang^{35,75} Shuihan Zhang^{1,58}, Shulei Zhang^{23,h}, X. D. Zhang⁴¹, X. M. Zhang¹, X. Y. Zhang⁴⁵, X. Y. Zhang⁵⁰, Y. Zhang⁶⁴, Y. T. Zhang⁷⁵, Y. H. Zhang^{1,58}, Yan Zhang^{53,66}, Yao Zhang¹, Z. H. Zhang¹, Z. Y. Zhang⁷¹, Z. Y. Zhang³⁹, G. Zhao¹, J. Zhao³⁵, J. Y. Zhao^{1,58}, J. Z. Zhao^{1,53}, Lei Zhao^{53,66}, Ling Zhao¹, M. G. Zhao³⁹, Q. Zhao¹, S. J. Zhao⁷⁵, Y. B. Zhao^{1,53}, Y. X. Zhao^{28,58}, Z. G. Zhao^{53,66}, A. Zhemchugov^{32,a}, B. Zheng⁶⁷, J. P. Zheng^{1,53}, Y. H. Zheng⁵⁸, B. Zhong³⁷, C. Zhong⁶⁷, X. Zhong⁵⁴, H. Zhou⁴⁵, L. P. Zhou^{1,58}, X. Zhou⁷¹, X. K. Zhou⁵⁸, X. R. Zhou^{53,66}, X. Y. Zhou³⁵, Y. Z. Zhou^{10,f}, J. Zhu³⁹, X. Zhou^{53,66}, X. Y. Zhou $\text{K. Zhu}^{1},\,\text{K. J. Zhu}^{1},\,\text{L. X. Zhu}^{58},\,\text{S. H. Zhu}^{65},\,\text{S. Q. Zhu}^{38},\,\text{T. J. Zhu}^{72},\,\text{W. J. Zhu}^{10,f},\,\text{Y. C. Zhu}^{53,66},\,\text{Z. A. Zhu}^{1,58},\,\text{Zhu}^{1,5$ B. S. Zou¹, J. H. Zou¹

(BESIII Collaboration) ¹ Institute of High Energy Physics, Beijing 100049, People's Republic of China ² Beihang University, Beijing 100191, People's Republic of China ³ Beijing Institute of Petrochemical Technology, Beijing 102617, People's Republic of China ⁴ Bochum Ruhr-University, D-44780 Bochum, Germany ⁵ Carnegie Mellon University, Pittsburgh, Pennsylvania 15213, USA ⁶ Central China Normal University, Wuhan 430079, People's Republic of China ⁷ Central South University, Changsha 410083, People's Republic of China ⁸ China Center of Advanced Science and Technology, Beijing 100190, People's Republic of China ⁹ COMSATS University Islamabad, Lahore Campus, Defence Road, Off Raiwind Road, 54000 Lahore, Pakistan ¹⁰ Fudan University, Shanghai 200433, People's Republic of China ¹¹ G.I. Budker Institute of Nuclear Physics SB RAS (BINP), Novosibirsk 630090, Russia ¹² GSI Helmholtzcentre for Heavy Ion Research GmbH, D-64291 Darmstadt, Germany ¹³ Guangxi Normal University, Guilin 541004, People's Republic of China ¹⁴ Guangxi University, Nanning 530004, People's Republic of China ¹⁵ Hangzhou Normal University, Hangzhou 310036, People's Republic of China ¹⁶ Hebei University, Baoding 071002, People's Republic of China ¹⁷ Helmholtz Institute Mainz, Staudinger Weg 18, D-55099 Mainz, Germany ¹⁸ Henan Normal University, Xinxiang 453007, People's Republic of China ¹⁹ Henan University of Science and Technology, Luoyang 471003, People's Republic of China ²⁰ Henan University of Technology, Zhengzhou 450001, People's Republic of China ²¹ Huangshan College, Huangshan 245000, People's Republic of China ²² Hunan Normal University, Changsha 410081, People's Republic of China ²³ Hunan University, Changsha 410082, People's Republic of China ²⁴ Indian Institute of Technology Madras, Chennai 600036, India ²⁵ Indiana University, Bloomington, Indiana 47405, USA ²⁶ (A)INFN Laboratori Nazionali di Frascati, I-00044, Frascati, Italy; (B)INFN Sezione di Perugia, I-06100, Perugia, Italy; (C) University of Perugia, I-06100, Perugia, Italy ²⁷ (A)INFN Sezione di Ferrara, I-44122, Ferrara, Italy; (B)University of Ferrara, I-44122, Ferrara, Italy

²⁸ Institute of Modern Physics, Lanzhou 730000, People's Republic of China ²⁹ Institute of Physics and Technology, Peace Avenue 54B, Ulaanbaatar 13330, Mongolia

³⁰ Jilin University, Changchun 130012, People's Republic of China

³¹ Johannes Gutenberg University of Mainz, Johann-Joachim-Becher-Weg 45, D-55099 Mainz, Germany ³² Joint Institute for Nuclear Research, 141980 Dubna, Moscow region, Russia

³³ Justus-Liebig-Universitaet Giessen, II. Physikalisches Institut, Heinrich-Buff-Ring 16, D-35392 Giessen, Germany ³⁴ Lanzhou University, Lanzhou 730000, People's Republic of China

> ³⁵ Liaoning Normal University, Dalian 116029, People's Republic of China ³⁶ Liaoning University, Shenyang 110036, People's Republic of China

> ³⁷ Nanjing Normal University, Nanjing 210023, People's Republic of China

```
38 Nanjing University, Nanjing 210093, People's Republic of China
                                <sup>39</sup> Nankai University, Tianjin 300071, People's Republic of China
                                <sup>40</sup> National Centre for Nuclear Research, Warsaw 02-093, Poland
                     <sup>41</sup> North China Electric Power University, Beijing 102206, People's Republic of China
                                <sup>42</sup> Peking University, Beijing 100871, People's Republic of China
                              <sup>43</sup> Qufu Normal University, Qufu 273165, People's Republic of China
                           <sup>44</sup> Shandong Normal University, Jinan 250014, People's Republic of China
                                <sup>45</sup> Shandong University, Jinan 250100, People's Republic of China
                        <sup>46</sup> Shanghai Jiao Tong University, Shanghai 200240, People's Republic of China
                            <sup>47</sup> Shanxi Normal University, Linfen 041004, People's Republic of China
                                <sup>48</sup> Shanxi University, Taiyuan 030006, People's Republic of China
                               <sup>49</sup> Sichuan University, Chengdu 610064, People's Republic of China
                               <sup>50</sup> Soochow University, Suzhou 215006, People's Republic of China
                      <sup>51</sup> South China Normal University, Guangzhou 510006, People's Republic of China
                              <sup>52</sup> Southeast University, Nanjing 211100, People's Republic of China
  <sup>53</sup> State Key Laboratory of Particle Detection and Electronics, Beijing 100049, Hefei 230026, People's Republic of China
                           <sup>54</sup> Sun Yat-Sen University, Guangzhou 510275, People's Republic of China
             <sup>55</sup> Suranaree University of Technology, University Avenue 111, Nakhon Ratchasima 30000, Thailand
                               <sup>56</sup> Tsinghua University, Beijing 100084, People's Republic of China
   <sup>57</sup> (A)Istinye University, 34010, Istanbul, Turkey; (B)Near East University, Nicosia, North Cyprus, Mersin 10, Turkey
                   <sup>58</sup> University of Chinese Academy of Sciences, Beijing 100049, People's Republic of China
                             <sup>59</sup> University of Groningen, NL-9747 AA Groningen, The Netherlands
                                      <sup>60</sup> University of Hawaii, Honolulu, Hawaii 96822, USA
                                <sup>61</sup> University of Jinan, Jinan 250022, People's Republic of China
                      <sup>62</sup> University of Manchester, Oxford Road, Manchester, M13 9PL, United Kingdom
                       <sup>63</sup> University of Muenster, Wilhelm-Klemm-Strasse 9, 48149 Muenster, Germany
                             <sup>64</sup> University of Oxford, Keble Road, Oxford OX13RH, United Kingdom
                <sup>65</sup> University of Science and Technology Liaoning, Anshan 114051, People's Republic of China
                  <sup>66</sup> University of Science and Technology of China, Hefei 230026, People's Republic of China
                          <sup>67</sup> University of South China, Hengyang 421001, People's Republic of China
                                       <sup>68</sup> University of the Punjab, Lahore-54590, Pakistan
<sup>69</sup> (A) University of Turin, I-10125, Turin, Italy; (B) University of Eastern Piedmont, I-15121, Alessandria, Italy; (C)INFN,
                                                        I-10125, Turin, Italy
                                   <sup>70</sup> Uppsala University, Box 516, SE-75120 Uppsala, Sweden
                                <sup>71</sup> Wuhan University, Wuhan 430072, People's Republic of China
                          <sup>72</sup> Xinyang Normal University, Xinyang 464000, People's Republic of China
                              <sup>73</sup> Yunnan University, Kunming 650500, People's Republic of China
                              <sup>74</sup> Zhejiang University, Hangzhou 310027, People's Republic of China
                            <sup>75</sup> Zhengzhou University, Zhengzhou 450001, People's Republic of China
                       <sup>a</sup> Also at the Moscow Institute of Physics and Technology, Moscow 141700, Russia
                             <sup>b</sup> Also at the Novosibirsk State University, Novosibirsk, 630090, Russia
                           <sup>c</sup> Also at the NRC "Kurchatov Institute", PNPI, 188300, Gatchina, Russia
                          <sup>d</sup> Also at Goethe University Frankfurt, 60323 Frankfurt am Main, Germany
<sup>e</sup> Also at Key Laboratory for Particle Physics, Astrophysics and Cosmology, Ministry of Education; Shanghai Key Laboratory
for Particle Physics and Cosmology; Institute of Nuclear and Particle Physics, Shanghai 200240, People's Republic of China
   f Also at Key Laboratory of Nuclear Physics and Ion-beam Application (MOE) and Institute of Modern Physics, Fudan
                                     University, Shanghai 200443, People's Republic of China
<sup>g</sup> Also at State Key Laboratory of Nuclear Physics and Technology, Peking University, Beijing 100871, People's Republic of
                                                                China
                   <sup>h</sup> Also at School of Physics and Electronics, Hunan University, Changsha 410082, China
   <sup>i</sup> Also at Guangdong Provincial Key Laboratory of Nuclear Science, Institute of Quantum Matter, South China Normal
                                               University, Guangzhou 510006, China
   <sup>j</sup> Also at Frontiers Science Center for Rare Isotopes, Lanzhou University, Lanzhou 730000, People's Republic of China
     <sup>k</sup> Also at Lanzhou Center for Theoretical Physics, Lanzhou University, Lanzhou 730000, People's Republic of China
                          l Also at the Department of Mathematical Sciences, IBA, Karachi, Pakistan
```

Abstract Using data taken at 29 center-of-mass energies between 4.16 and 4.70 GeV with the BESIII detector at the Beijing Electron Positron Collider corresponding to a total integrated luminosity of approximately 18.8 fb⁻¹, the process $e^+e^- \to pp\bar{p}\bar{n}\pi^- + c.c.$ is observed for the first time with a statistical significance of 11.5 σ . The average Born cross sections in the energy ranges of (4.160, 4.380) GeV, (4.400, 4.600) GeV and (4.610, 4.700) GeV are measured to be (21.5 \pm 5.7 \pm 1.2) fb, (46.3 \pm 10.6 \pm 2.5) fb and (59.0 \pm 9.4 \pm 3.2) fb, respectively, where the first uncertainties are

statistical and the second are systematic. The line shapes of the $\bar{p}\bar{n}$ and $pp\pi^-$ invariant mass spectra are consistent with phase space distributions, indicating that no hexaquark or di-baryon state is observed.

Key words Multi-baryon channel, hexaquark, di-baryon states, cross section measurement

1 INTRODUCTION

One of the most fundamental questions in hadron physics is related to the mechanism of color confinement in Quantum Chromodynamics (QCD). Colorsinglet hadronic configurations of quarks and gluons can form bound states or resonances. Besides the well-known combinations of $q\bar{q}$ for mesons and qqq for baryons, other combinations, such as $gq\bar{q}$ for hybrid states [1], multi-gluons for glueball states [2], $q\bar{q}q\bar{q}$ for tetraquark states [3], $qqqq\bar{q}$ for pentaguark states [4] and hexaguark states (qqqqqq), are also allowed by QCD. Di-baryon and hexaquark states have been searched for in a range of nucleon-nucleon scattering reactions. Recently, an isoscalar resonant structure was observed in the isoscalar two-pion fusion process $pn \to d\pi^0\pi^0$ [5] by the WASA Collaboration and was later confirmed in the other twopion fusion processes $pn \to d\pi^+\pi^-$ [6] and $pp \to d\pi^+\pi^0$ [7], and the two-pion non-fusion process $pn \to pp\pi^0\pi^-$ [8] and $pn \to pn\pi^0\pi^0$ [9]. This state was denoted by $d^*(2380)$ following the convention used for nucleon excitations. These observations indicate the possibility of the existence of hexaquark and di-baryon configurations. In 2021, the BESIII Collaboration reported the search for hexaquark and di-baryon states in examining the invariant mass spectra of two baryons in the process $e^+e^- \rightarrow 2(p\bar{p})$ [10], and no significant signal was observed.

Analyzing data sets corresponding to a total integrated luminosity of approximately 18.8 fb⁻¹ taken at center-of-mass energies \sqrt{s} between 4.16 and 4.70 GeV with the BESIII detector, we present in this paper the first measurement of the cross section of the process $e^+e^- \to pp\bar{p}\bar{n}\pi^- + c.c.$. We search for the $d^*(2380)$ and other possible hexaquark or di-baryon states with the data samples with energies above 4.60 GeV, where the $\bar{p}\bar{n}$ system with a mass around 2.4 GeV for $d^*(2380)$ is kinematically accessible. The mass range of the $\bar{p}\bar{n}$ system around 2.4 GeV/ c^2 , in which the $d^*(2380)$ might contribute, is covered by the data samples with energies above 4.60 GeV. Throughout this paper, charge conjugation is always implied unless explicitly stated, and in discussing systematic uncertainties.

2 THE BESIII DETECTOR AND DATA SAMPLES

The BESIII detector [11] records symmetric e^+e^- collisions provided by the BEPCII storage ring [12], which operates in the center-of-mass energy range from 2.0 to 4.95 GeV. BESIII has collected large data samples in this energy region [13]. The cylindrical core of the BESIII detector covers 93% of the full solid angle and consists of a helium-based multilayer drift chamber (MDC), a plastic

scintillator time-of-flight system (TOF), and a CsI(Tl) electromagnetic calorimeter (EMC), which are all enclosed in a superconducting solenoidal magnet providing a 1.0 T magnetic field. The solenoid is supported by an octagonal flux-return yoke with resistive plate counter muon identification modules interleaved with steel. The charged-particle momentum resolution at 1 GeV/c is 0.5%, and the specific energy loss (dE/dx) resolution is 6% for electrons from Bhabha scattering. The EMC measures photon energies with a resolution of 2.5% (5%) at 1 GeV in the barrel (end cap) region. The time resolution in the TOF barrel region is 68 ps, while that in the end cap region is 110 ps. The end cap TOF system was upgraded in 2015 using multi-gap resistive plate chamber technology, providing a time resolution of 60 ps [14].

The data sets were collected at 29 center-of-mass energies between 4.16 and 4.70 GeV. The nominal energies of the data sets from 4.16 to 4.60 GeV are measured by the di-muon process $e^+e^- \to (\gamma_{\rm ISR/FSR})\mu^+\mu^-$ [15, 16], where the subscript ISR/FSR stands for the initial-state or final-state radiation process, respectively. The data sets from 4.61 to 4.70 GeV are calibrated by the process $e^+e^- \to \Lambda_c^+\bar{\Lambda}_c^-$ [17]. The integrated luminosity $\mathcal{L}_{\rm int}$ is determined using large-angle Bhabha scattering events [17, 18]. The total integrated luminosity of all data sets is approximately 18.8 fb⁻¹.

The response of the BESIII detector is modeled with Monte Carlo (MC) simulations using the software framework BOOST [19] based on GEANT4 [20], which includes the geometry and material description of the BESIII detector, the detector response and digitization models, as well as a database that keeps track of the running conditions and the detector performance. Large MC simulated event samples are used to optimize the selection criteria, evaluate the signal efficiency, and estimate background contributions.

Inclusive MC simulation samples are generated at different center-of-mass energies to study potential background reactions. These samples consist of open charm processes, the ISR production of vector charmonium and charmonium-like states, and the continuum processes incorporated in KKMC [21]. The known decay modes are modeled with EVTGEN [22] using branching fractions taken from the Particle Data Group (PDG) [23], and the remaining unknown decays of the charmonium states are simulated with LUNDCHARM [24]. Final-state radiation from charged final-state particles is incorporated with PHOTOS [25]. The signal MC simulation sample of $e^+e^- \to pp\bar{p}\bar{n}\pi^-$ at each energy point is generated with the events being uniformly distributed in phase space.

3 DATA ANALYSIS

Events with two positive and two negative charged tracks are selected. For each charged track, the polar angle in the MDC with respect to the z direction must satisfy $|\cos\theta| < 0.93$. All charged tracks are required to originate from the interaction region, defined as $R_{xy} < 1$ cm and $|V_z| < 10$ cm, where R_{xy} and $|V_z|$ are the distances from the point of closest approach of the tracks to the interaction point in the x-y plane and in the z direction, respectively. The combined $\mathrm{d}E/\mathrm{d}x$ and TOF information are used to calculate particle identification (PID) confidence levels for the pion, kaon, and proton hypotheses. Each track is assigned as the particle hypothesis with the highest confidence level. The final state in the $e^+e^- \to pp\bar{p}\bar{n}\pi^-$ process is reconstructed with three (anti)protons and one π^- .

Since the neutron can not be well reconstructed with the BESIII detector, the signal process is determined via the recoiling mass of the reconstructed charged particles, defined as

$$M_{\rm rec}c^2 = \sqrt{(E_{e^+e^-} - E_{pp\bar{p}\pi^-})^2 - (\vec{P}_{e^+e^-} - \vec{P}_{pp\bar{p}\pi^-})^2 \cdot c^2},$$
(1)

where $E_{e^+e^-}$ and $\vec{P}_{e^+e^-}$ are the center-of-mass energy and the momentum of the e^+e^- system, respectively; $E_{pp\bar{p}\pi^-}$ and $\vec{P}_{pp\bar{p}\pi^-}$ are the total reconstructed energy and total momentum of the $pp\bar{p}\pi^-$ system, respectively. Events with $M_{\rm rec}$ greater than 0.8 GeV/ c^2 are kept for further analysis.

Studies based on the inclusive MC simulation samples [26] show that no peaking background events survive the selection criteria. To further suppress background events, two additional selection criteria are imposed on the accepted candidate events. First, the invariant mass $M_{p\pi^-}$ of the reconstructed $p\pi^-$ system is required to be outside the Λ signal region, i.e. $|M_{p\pi^-}-1.115|>0.010$ GeV/ c^2 , to remove the possible background associated with Λ decays. Here, 1.115 GeV/ c^2 is the known Λ mass [29], and 0.010 GeV/ c^2 corresponds to about three times the mass resolution. Second, the invariant mass of $pp\bar{p}$ ($M_{pp\bar{p}}$) must be less than 3.6 GeV/ c^2 due to the remaining neutron and pion in the event.

The $M_{\rm rec}$ distribution of the accepted candidates after the above selection criteria from the combined data sets is displayed in Fig. 1, where a significant neutron signal is observed. The signal yield is determined by a maximum likelihood fit to this distribution. In the fit, the signal is represented by the luminosity weighted MC-simulated shape convolved with a Gaussian function and the remaining background is described by a linear function. From the fit, the signal yield is determined to be 123 ± 14 . The statistical significance of the signal is determined to be 11.5σ , which is evaluated as $\sqrt{-2\ln(\mathcal{L}_0/\mathcal{L}_{\rm max})}$, where $\mathcal{L}_{\rm max}$ is the maximum likelihood of the nominal fit and \mathcal{L}_0 is the likelihood of the fit without involving the signal component. The change of the degree of freedom is 1. The neutron signal region is de-

fined as $M_{\rm rec} \in (0.925, 0.968)~{\rm GeV}/c^2$ and the corresponding sideband regions are defined as $M_{\rm rec} \in (0.857, 0.900)$ $\cup (0.990, 1.033)~{\rm GeV}/c^2$.

Figure 2 shows the comparisons of the momentum and polar angle distributions of the neutron of the accepted candidate events between data and signal MC simulation samples, where the data distribution is from the combined data sets and the MC simulation distribution has been weighted by the signal yields in data. The invariant mass of any two or three particles, the momentum and $\cos\theta$ distributions of the other final state particles have also been examined. The agreement between data and MC simulation allows to determine the detection efficiency with the signal MC simulation events generated uniformly distributed in the five-body phase space.

To search for hexaquark and di-baryon states, the $\bar{p}\bar{n}$ invariant mass spectrum is examined. Figure 3 shows the $pp\pi^-$ and $\bar{p}\bar{n}$ invariant mass spectra of the candidate events for the reaction $e^+e^-\to pp\bar{p}\bar{n}\pi^-$. In the fit to $M_{\bar{p}\bar{n}}$, the signal is represented by the luminosity weighted phase space MC simulation shape and the remaining combinatorial background is described by a linear function. The goodness-of-fit is $\chi^2/ndf=2.10/2$. Here, ndf is the number of degrees of freedom. Compared to the phase space hypothesis, no obvious structure is observed.

4 AVERAGE CROSS SECTIONS

In each data set, only a few events have been observed in the neutron signal region, with a statistical significance of less than 3σ . To obtain significant neutron signals the data sets are combined into three sub-samples in the energy ranges of (4.160, 4.380), (4.400, 4.600) and (4.610, 4.700) GeV for further analysis.

The average observed cross section for $e^+e^- \rightarrow pp\bar{p}\bar{n}\pi^-$ is calculated by

$$\overline{\sigma}_{j}^{\text{obs}} = \frac{N_{j}^{\text{sig}}}{\sum_{i} \epsilon_{ij} \cdot \mathcal{L}_{ij}}, \tag{2}$$

where $N_j^{\rm sig}$ is the number of signal events from the j-th combined data set, \mathcal{L}_i and ϵ_i are the integrated luminosity and efficiency of data set i, respectively, i represents the i-th energy point in j-th sub-data set. The detection efficiency is corrected by the PID and tracking efficiencies correction factors, $f_{\rm PID}$ and $f_{\rm trk}$, which are determined to be 0.92 and 0.98 by weighting the differences between data and MC simulation efficiencies in different momentum ranges, respectively. Inserting the numbers which are listed in Table 1 into Eq. 2 yields the average observed cross sections $(19.4\pm5.1\pm1.0)$ fb, $(42.8\pm9.8\pm2.3)$ fb and $(54.2\pm8.6\pm2.9)$ fb for the three sub-data sets, respectively, where the first uncertainties are statistical and the second are systematic.

To measure the average Born cross section of $e^+e^- \rightarrow pp\bar{p}\bar{n}\pi^-$, a similar lineshape as that of $e^+e^- \rightarrow 2(p\bar{p})$ [10] is assumed to determine the ISR and vacuum polariza-

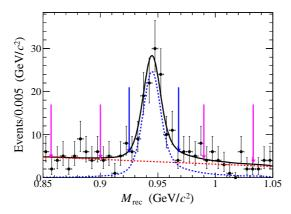


Figure 1. Distribution of the recoiling mass $M_{\rm rec}$ of the candidate events for the reaction $e^+e^- \to pp\bar{p}\bar{n}\pi^-$ with the fit results overlaid. The dots with error bars are from the combined data sets, the black curve shows the total fit result, and the dashed blue (red) curve represents the signal (background) shape. The pair of blue arrows marks the neutron signal region, whereas the neutron sideband regions are visualized by the two pairs of pink arrows.

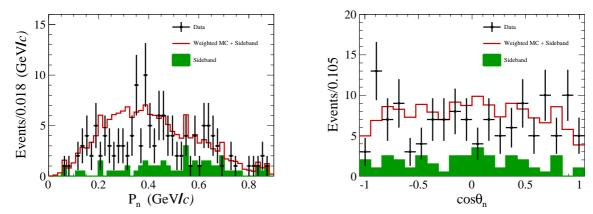


Figure 2. Momentum (left) and polar angular distributions (right) of the neutrons of the candidate events for the reaction $e^+e^- \to pp\bar{p}\bar{n}\pi^-$. The dots with error bars represent the combined data sets. The green histograms represent the sideband events. The red histograms represent the weighted signal MC simulation events plus the normalized neutron sideband regions in data.

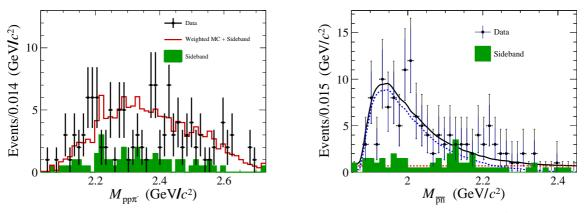


Figure 3. The $pp\pi^-$ (left) and $\bar{p}\bar{n}$ (right) invariant mass spectra of the candidate events for $e^+e^- \to pp\bar{p}\bar{n}\pi^-$. The dots with error bars represent the combined data sets. The green histograms are the normalized neutron sideband events in data. The red histograms represent the weighted signal MC simulation events plus the normalized neutron sideband events in data. The black solid curve shows the total fit result, the blue dashed curve is the signal shape derived from the signal MC simulation sample, and the red dashed line is the linear background shape.

tion correction factors, $(1 + \delta^{\gamma})$ and $\frac{1}{|1 - \Pi|^2}$, as they are similar reactions where one of the \bar{p} has been exchanged

by $\bar{n}\pi^-$. The average Born cross section is calculated by

$$\overline{\sigma}_{j}^{\text{Born}} = \frac{\overline{\sigma}_{j}^{\text{obs}}}{(1 + \delta^{\gamma})_{j} \cdot \left(\frac{1}{|1 - \Pi|^{2}}\right)_{j}}.$$
 (3)

The obtained Born cross sections are then used as input in the generator and the cross section measurements are iterated with the updated detection efficiencies. This process is repeated until the $(1+\delta^{\gamma})\cdot\epsilon$ values become stable at all energies, i.e. the difference of $(1+\delta^{\gamma})\cdot\epsilon$ between the last two iterations is less than 4%. Figure 4 shows the obtained average Born cross sections in the defined subsamples. The average Born observed cross sections are calculated with Eq. 3, and the results are $(21.5\pm5.7\pm1.2)$ fb, $(46.3\pm10.6\pm2.5)$ fb and $(59.0\pm9.4\pm3.2)$ fb for the three sub-data sets, respectively, where the first uncertainties are statistical and the second are systematic. Two different functions are used to compare the trend of the average Born cross section to a reaction where a similar behaviour is expected. The first one is a simple five-body energydependent phase space lineshape [10, 27] and the second one is an exponential function [10, 28], which are shown in Figure 4. The exponential function is constructed as

$$\sigma^{\text{Born}}(s) = \frac{1}{s} \times e^{-p_0(\sqrt{s} - M_{\text{th}})} \times p_1, \tag{4}$$

where p_0 and p_1 are free parameters, $M_{\rm th}=(3m_p+m_n+m_{\pi^-}),\ m_p,\ m_n,$ and m_{π^-} are the known masses of $p,\ n,$ and π^- taken from the PDG [29]. This is similar to the one used for the cross section lineshape of $e^+e^- \to 2(p\bar{p})$ in Ref. [10], as they are similar reactions where one of the \bar{p} has been exchanged by $\bar{n}\pi^-$. However, it should be noted that the two functions in Figure 4 are not fit results, but drawn with arbitrary scale factors for comparison since a qualitative fit is not possible due to the limited statistics.

The systematic uncertainties in the cross section measurements will be discussed in the next section.

5 SYSTEMATIC UNCERTAINTY

In the cross section measurements, the systematic uncertainties mainly comes from the integrated luminosity, tracking efficiency, PID efficiency, ISR correction, $M_{\rm rec}$ fit, and veto of background events associated with Λ decays.

The integrated luminosity of the data set is measured by large-angle Bhabha scattering events, and the uncertainty in the measurement is 1.0% [18], which is dominated by the precision of the MC generator used for efficiency correction. The tracking and PID efficiencies have been studied with high purity control samples of $J/\psi \to p\bar{p}\pi^+\pi^-$ and $\psi(3686) \to \pi^+\pi^-J/\psi \to \pi^+\pi^-p\bar{p}$ decays [30, 31]. The differences of the tracking and PID efficiencies between data and MC simulation in different transverse momentum and total momentum ranges are obtained separately. The averaged differences for the tracking (PID) efficiencies are corrected by the factors f_{trk} (f_{PID}) as mentioned in Sec. 4. The uncertainties of the tracking and PID efficiencies are reweighted by the p/\bar{p} and π^+/π^- momenta of the signal MC simulation events. The reweighted uncertainties for tracking (PID) efficiencies, 0.1% (0.3%) per p, 0.1% (0.4%) per \bar{p} , 1.0%

(0.5%) per π^+ and 0.8% (0.4%) per π^- , are assigned as the systematic uncertainties. Adding them linearly gives the total systematic uncertainties due to the tracking and PID efficiencies to be 1.1% and 1.6% for the process $e^+e^- \to pp\bar{p}\bar{n}\pi^-$, and 1.3% and 1.9% for the process $e^+e^- \to p\bar{p}\bar{p}n\pi^+$, respectively.

The input Born cross sections in the generator are iterated until the $(1+\delta^{\gamma}) \cdot \epsilon$ values converge. The largest difference of $(1+\delta^{\gamma}) \cdot \epsilon$ between the last two iterations at all energy points, 3.2%, is taken as the corresponding systematic uncertainty.

Three different tests were performed to estimate the uncertainty associated with the $M_{\rm rec}$ fit. The fit range is increased or decreased by 5 MeV/ c^2 . The background shape is replaced with a second-order Chebychev polynomial function, and the signal shape is replaced with an MC simulation-derived shape convolved with a Gaussian function. The quadrature sum of these changes, 3.6%, is taken as the relevant uncertainty.

The systematic uncertainty due to the veto of Λ background events is estimated by changing the Λ veto mass window from $\pm 3\sigma$ to $\pm 5\sigma$, where σ is the invariant mass resolution and the value is 3 MeV/ c^2 . The change of the measured cross section, 0.03%, is assigned as the uncertainty.

Adding the above systematic uncertainties summarized in Table 2 in quadrature yields the total systematic uncertainties of 5.3% and 5.4%, for the processes $e^+e^- \to pp\bar{p}\bar{n}\pi^-$ and $e^+e^- \to p\bar{p}\bar{p}n\pi^+$, respectively. The average systematic uncertainty, 5.35%, is taken as the total systematic uncertainty in the cross section measurement for the process $e^+e^- \to pp\bar{p}\bar{n}\pi^- + c.c.$.

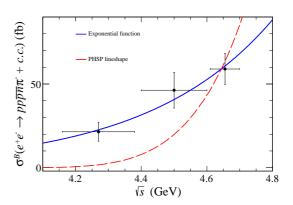


Figure 4. Average Born cross sections for the process $e^+e^- \to pp\bar{p}\bar{n}\pi^- + c.c.$. The dots with error bars are the measured values, the blue line shows the exponential function curve and the red-dashed line shows the five-body energy-dependent phase spase (PHSP) lineshape curve.

Table 1. The average observed cross sections for the reaction $e^+e^- \to pp\bar{p}\bar{n}\pi^- + c.c.$. Summary of the number of signal events $(N_{\rm sig})$, integrated luminosity (\mathcal{L}) , detection efficiency (ϵ) , radiative correction factors $(1+\delta^{\gamma})$, the average observed cross section $(\overline{\sigma}^{\rm obs})$ and average Born cross section $(\overline{\sigma}^{\rm Born})$ at different c.m. energies (\sqrt{s}) . The uncertainties are statistical only.

 $\sqrt{s} \; (\mathrm{GeV})$	\mathcal{L} (pb ⁻¹)	ϵ (%)	$(1+\delta^{\gamma})$	$N_{ m sig}$	$\overline{\sigma}^{\mathrm{obs}}$ (fb)	$\overline{\sigma}^{\mathrm{Born}}$ (fb)
4.1574	408.70	4.2	0.8408		19.4 ± 5.1	21.5 ± 5.7
4.1780	3189.0	6.0	0.8388			
4.1889	526.70	7.1	0.8430			
4.1990	526.00	8.1	0.8456			
4.2092	517.10	8.8	0.8485			
4.2188	514.60	9.6	0.8509			
4.2263	1056.40	10.1	0.8489			
4.2358	530.30	11.4	0.8530			
4.2439	538.10	12.0	0.8552	22.7 ± 6.0		
4.2580	828.40	13.5	0.8559			
4.2668	531.10	14.0	0.8587			
4.2777	175.70	14.8	0.8593			
4.2878	502.40	14.2	0.8612			
4.3121	501.20	16.2	0.8628			
4.3374	505.00	18.6	0.8646			
4.3583	543.90	21.8	0.8693			
4.3774	522.70	21.0	0.8668			
 4.3965	507.80	22.6	0.8674		42.8±9.8	46.3 ± 10.6
4.4156	1043.90	24.8	0.8764			
4.4362	569.90	25.0	0.8683	30.9 ± 7.1		
4.4671	111.09	27.4	0.8794	30.9±1.1		
4.5271	112.12	30.7	0.8838			
4.5995	586.90	34.0	0.8876			
 4.6152	103.83	33.5	0.8712		54.2±8.6	59.0 ± 9.4
4.6304	521.52	34.1	0.8710	69.4 ± 11.0		
4.6431	552.41	34.5	0.8708			
4.6639	529.63	35.7	0.8712	03.4 ± 11.0		
4.6842	1669.31	36.3	0.8711			
4.7008	536.45	36.6	0.8710			

Table 2. The relative systematic uncertainties (in %) from the integrated luminosity of data set (\mathcal{L}) , the tracking efficiency (Trk), the PID efficiency (PID), the ISR correction (ISR), the $M_{\rm rec}$ fit (Fit), and the Λ veto in the cross section measurements.

Mode	\mathcal{L}	Trk	PID	ISR	Fit	Λ veto	Total
$pp\bar{p}\bar{n}\pi^-$	1.0	1.1	1.6	3.2	3.6	0.03	5.3
$p\bar{p}\bar{p}n\pi^+$	1.0	1.3	1.9	3.2	3.6	0.03	5.4

6 SUMMARY

By using the data sets taken at the center-of-mass energies between 4.16 and 4.70 GeV, the process $e^+e^- \rightarrow pp\bar{p}\bar{n}\pi^- + c.c.$ has been observed for the first time with a statistical significance of 11.5σ . The average Born

cross sections in the three energy ranges of (4.160, 4.380), (4.400, 4.600) and (4.610, 4.700) GeV are measured to be (21.5 \pm 5.7 \pm 1.2) fb, (46.3 \pm 10.6 \pm 2.5) fb and (59.0 \pm 9.4 \pm 3.2) fb, respectively, where the first uncertainties are statistical and the second systematic. The Born cross section close to threshold is larger than would be expected from five-body phase space. The lineshape of the average Born cross sections for the process $e^+e^- \to pp\bar{p}\bar{n}\pi^- + c.c.$ shows similar behaviour to that of the process $e^+e^- \to 2(p\bar{p})$. The shape of the invariant-mass spectra of $\bar{p}\bar{n}$ and $pp\pi^-$ are in good agreement with the phase-space distributions, thereby indicating no hexaquark or di-baryon state observed with the current data sample size.

The BESIII collaboration thanks the staff of BEPCII and the IHEP computing center for their strong support.

References

```
1 E. Braaten, C. Langmack, D. Hudson Smith, Phys. Rev. D 90, 014044 (2014).
 2 C. J. Morningstar and M. J. Peardon, Phys. Rev. D 60, 034509 (1999).
 3 M. Ablikim et al. (BESIII Collaboration), Phys. Rev. Lett. 110, 252001 (2013).
 4 R. Aaij et al. (LHCb Collaboration), Phys. Rev. Lett. 115, 072001 (2015).
 5 M. Bashkanov et al. (CELSIUS/WASA Collaboration), Phys. Rev. Lett. 102, 052301 (2009).
 6 P. Adlarson et al. (WASA-at-COSY Collaboration), Phys. Rev. Lett. 106, 242302 (2011).
 7 F. Kren et al. (CELSIUS/WASA Collaboration), Phys. Lett. B 684, 110 (2010), Erratum: Phys. Lett. B 702, 312 (2011).
 8 P. Adlarson et al. (WASA-at-COSY Collaboration), Phys. Rev. C 88, 055208 (2013).
9 P. Adlarson et al. (WASA-at-COSY Collaboration), Phys. Lett. B 743, 325 (2015).
10 M. Ablikim et al. (BESIII Collaboration), Phys. Rev. D 103, 052003 (2021).
   M. Ablikim et al. (BESIII Collaboration), Nucl. Instrum. Meth. A 614, 345 (2010).
12 C. H. Yu et al., Proceedings of IPAC2016, Busan, Korea, 2016, doi: 10.18429/JACoW-IPAC2016-TUYA01.
13 M. Ablikim et al. (BESIII Collaboration), Chin. Phys. C 44, 040001 (2020).
14 X. Li et al., Radiat. Detect. Technol. Methods 1, 13 (2017);
    Y. X. Guo et al., Radiat. Detect. Technol. Methods 1, 15 (2017).
15 M. Ablikim et al. (BESIII Collaboration), Chin. Phys. C 40, 063001 (2016).
16 M. Ablikim et al. (BESIII Collaboration), Chin. Phys. C 45, 103001 (2021).
   M. Ablikim et al. (BESIII Collaboration), Publication in preparation.
18 M. Ablikim et al. (BESIII Collaboration), Submitted to Chin. Phys. C, arXiv:2203.03133 [hep-ex].
19 Z. Y. Deng et al., High Energy Physics & Nuclear Physics. 30, 371 (2006).
20 S. Agostinelli et al. (GEANT4 Collaboration), Nucl. Instrum. Meth. A 506, 250 (2003).
21 S. Jadach, B. F. L. Ward, and Z. Was, Comput. Phys. Commun. 130, 260 (2000); Phys. Rev. D 63, 113009 (2001).
22 R. G. Ping, Chin. Phys. C 32, 599 (2008); D. J. Lange, Nucl. Instr. Meth. A 462, 152 (2001).
23 J. Beringer et al. (Particle Data Group), Phys. Rev. D 86, 010001 (2012) and 2013 partial update for the 2014 edition.
24 J. C. Chen, G. S. Huang and X. R. Qi et al., Phys. Rev. D 62, 034003 (2000);
    R. L. Yang, R. G. Ping and D. Chen, Chin. Phys. Lett. 31, 061301 (2014).
25 E. Richter-Was, Phys. Lett. B 303, 163 (1993).
26 X. Y. Zhou, S. X. Du, G. Li and C. P. Shen, Comput. Phys. Commun. 258, 107540 (2021)
27 E. Byckling and K. Kajantie, Particle Kinematics (Wiley, New York, 1973).
28 M. Ablikim et al. (BESIII Collaboration), Phys. Rev. Lett. 118, 092001 (2017).
29 M. Tanabashi et al. (Particle Data Group), Prog. Theor. Exp. Phys. 2020, 083C01 (2020).
30 M. Ablikim et al. (BESIII Collaboration), Phys. Rev. D 91, 112004 (2015).
31 M. Ablikim et al. (BESIII Collaboration), Phys. Rev. D 99, 031101 (2019).
```